HHS Public Access

Author manuscript

ACS Nano. Author manuscript; available in PMC 2019 February 13.

Published in final edited form as:

ACS Nano. 2018 July 24; 12(7): 6536–6544. doi:10.1021/acsnano.8b00553.

Mesenchymal Stem Cell/Red Blood Cell-Inspired Nanoparticle Therapy in Mice with Carbon Tetrachloride-Induced Acute Liver Failure

Hongxia Liang[†,‡,§,∇], **Ke Huang**[‡,§,∇], **Teng Su**[‡,§,∇], **Zhenhua Li**[‡,§,∥,∇], **Shiqi Hu**[‡,§], **Phuong-Uyen Dinh**[‡,§], **Emily A. Wrona**[§], **Chen Shao**[⊥], **Li Qiao**[‡,§,#], **Adam C. Vandergriff**[‡,§], **M. Taylor Hensley**[‡,§], **Jhon Cores**[‡,§], **Tyler Allen**[‡], **Hongyu Zhang**[†], **Qinglei Zeng**[†], **Jiyuan Xing**[†], **Donald O. Freytes**[§], **Deliang Shen**[†], **Zujiang Yu**[*,†], and **Ke Cheng**[*,†,‡,§]

[†]The First Affiliated Hospital of Zhengzhou University, Zhengzhou, Henan 450052, China

[‡]Department of Molecular Biomedical Sciences and Comparative Medicine Institute, North Carolina State University, Raleigh, North Carolina 27607, United States

[§]Joint Department of Biomedical Engineering and Comparative Medicine Institute, University of North Carolina at Chapel Hill and North Carolina State University, Chapel Hill and Raleigh, North Carolina 27599 and 27607, United States

[∥]College of Chemistry and Environmental Science, Chemical Biology Key Laboratory of Hebei Province, Analytical Chemistry Key Laboratory of Hebei Province, Key Laboratory of Medicinal Chemistry and Molecular Diagnosis of the Ministry of Education, Hebei University, Baoding, Hebei 071002, China

[⊥]Department of Pathology, China-Japan Friendship Hospital, Peking 100029, China

[#]Department of Cardiology, The Second Hospital of Hebei Medical University, Shijiazhuang, Hebei 050000, China

Abstract

Acute liver failure is a critical condition characterized by global hepatocyte death and often time needs a liver transplantation. Such treatment is largely limited by donor organ shortage. Stem cell therapy offers a promising option to patients with acute liver failure. Yet, therapeutic efficacy and feasibility are hindered by delivery route and storage instability of live cell products. We fabricated a nanoparticle that carries the beneficial regenerative factors from mesenchymal stem cells and further coated it with the membranes of red blood cells to increase blood stability. Unlike uncoated nanoparticles, these particles promote liver cell proliferation *in vitro* and have lower internalization by macrophage cells. After intravenous delivery, these artificial stem cell analogs are able to remain in the liver and mitigate carbon tetrachloride-induced liver failure in a mouse model, as

[*]**Corresponding Authors:** johnyuem@zzu.edu.cn, Ke_Cheng@ncsu.edu.

[∇]Author Contributions

H.L., K.H., T.S., and Z.L. contributed equally to this work. H.L, D.S., Z.Y., and K.C. conceived the study. K.H., T.S., Z.L., S.H., P.U., E.W., C.S., A.V., M.H., J.C, T.A., and D.F. performed the experiments and collected data. H.L., H.Z., Q.Z., J.X., and K.C. wrote the paper; H.L. and K.C. provided financial support.

Notes

The authors declare no competing financial interest.

gauged by histology and liver function test. Our technology provides an innovative and off-the-shelf strategy to treat liver failure.

Graphical Abstract

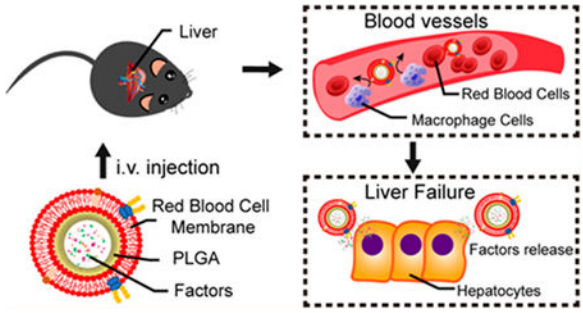

Keywords

mesenchymal stem cells; red blood cells; biomimetic; nanoparticles; membrane cloaking; liver failure

Acute liver failure, which follows an initial insult such as infection and toxic reagents, is a lethal condition characterized by global hepatocyte necrosis, acute deterioration of liver function, and subsequent multi-organ failure.[1] Orthotopic liver transplantation is currently viewed as the most effective treatment option for liver failure, but its use is limited by donor availability and the requirement for lifelong immunosuppression.[2,3] Therefore, alternative therapeutic and regenerative strategies for acute liver failure are urgently needed.[4]

Stem cell therapy offers an alternative strategy for treating hepatic diseases.[5] It has been shown that mesenchymal stem cells (MSCs) or MSC-derived microvesicles are able to mitigate acute liver failure in various animal models and in recently completed human trials.[6–8] However, cell therapy suffers several limitations. First, as a “live drug”, stem cell products need to be freshly prepared or carefully cryo-stored before final formulation. Moreover, due to their sizes, intravenously infused MSCs will be filtered by the lungs before they can reach the targeted organ (the liver). Portal vein injection can deliver a good amount of cells to the liver yet this method is invasive and repeated dosing is difficult. Numerous studies indicate that MSCs produce their functional benefits mainly through paracrine effects, that is, secreted factors from MSCs promote healing and inhibit fibrosis and inflammation.[9] We have previously fabricated therapeutic cell-mimicking particles by encapsulating MSC-secreted factors in a biodegradable polymer shell and tested their regenerative potential in a rodent model of heart injury.[10]

In recent years, there has been a tremendous success in the development of cell membrane-coated nanoparticles (NPs).[11,12] The membranes from various cell types empower NPs with functionalities that have been created and perfected by the nature, such as excellent stability in the blood.[13–15] For instance, it has been reported that NPs coated with the membranes of red blood cells (RBCs) can preserve the membrane protein complexes that are essential for

long blood circulation of RBCs,[16] prolonging the blood half-life of those NPs and amplifying their therapeutic effects.[17]

Based on these concepts, we designed a MSC/RBC-inspired nanoparticle (or MRIN). In summary, MRIN has a MSC core and a RBC shell. The MSC core is consisted of the therapeutic MSC secretome, encapsulated in a poly(lactic-*co*-glycolic acid) (PLGA). To increase stability, we further encased this particle in RBC membranes to make the final MRIN product. In the present study, we fabricated MRINs and tested their stability, biodistribution, and therapeutic potency in a murine model of acute liver failure.

RESULTS

Fabrication and Characterization of MRINs.

The schematic design of MRINs summarized in Figure 1A. The identity of MSCs was characterized by flow cytometry on common MSC markers (Figure 1B). In brief, MSC conditioned media (CM) was incorporated in PLGA to form nanoparticles (NPs or MSC-NPs) first. After that, the NPs were further coated with RBC cell membrane vesicles to form the final product MSC/RBC-inspired nanoparticle (MRIN). Transmission electron microscopy (TEM) imaging confirmed the RBC membrane coat on MRINs but not on NPs (Figure 2A,B). NanoSight characterization revealed that the size of MRIN was around 200 nm (Figure 2C,F). After RBC membrane cloaking, the size of NP did not change significantly (Figure 2C), while the ζ potential of MRIN changed from −47 to −10 mV (Figure 2D), in line with previously reported RBC NPs.[11] Overall, this “slightly negative” ζ potential is ideal for intravenous applications. Cryo-preservation did not alter the morphology, size, or ζ potential of MRINs (Figure 2G,H,J). MRINs were stable after long-term storage at room temperature, without significant coaggregation (Figure 2I). SDS-PAGE revealed similar protein compositions of RBC membranes and MRINs, further confirming successful RBC coating on MRINs (Figure 2E). Intravenously injected MIRN has a longer blood retention than NP in mice with acute liver failure (Figure 2K). The release profiles of growth factors such as insulin-like growth factor-1 (IGF), stromal cell-derived factor-1 (SDF-1), and hepatocyte growth factor (HGF) (Figure 2L) were indistinguishable between MRINs and control NPs. This indicates the RBC coating did not affect growth factor releases from MRINs.

MRINs Promote Liver Cell Proliferation while Discouraging Macrophage Uptake.

We tested the effects of co-culturing MRIN particles on various cell types *in vitro*, namely THLE-2 liver cells, HSC-T6 cells (rodent hepatic stellate cell line), and mouse lung cells (Figure 3A−C). CCK-8 cell proliferation assay revealed that MRINs promote the growth of THLE-2 liver cells (Figure 3D) with a dose-responsive manner. In contrast, co-culture with MRINs suppressed the proliferation of HSC-T6 cells (Figure 3E) and had no effects on mouse lung cells (Figure 3F). To test whether the RBC coat on MRINs increases the stability of the NPs by discouraging macrophage uptake, we co-cultured M1 macrophage cells with control (noncoated NPs) or MRINs. After 3 h of co-incubation, ~80% of NPs were taken up by macrophages, while only ~20% of MRINs were endocytosed (Figure 3G−J). This was further confirmed by *in vivo* studies, indicating minimal internalization of MRINs (red) by

liver macrophage cells (CD45, green) after intravenous injection (Figure 3K). Despite some uptake by liver cells, a large amount of MRINs remained in the extracellular space (Figure 3L).

Biodistribution of MRINs in Mice with Liver Failure.

To test the therapeutic potential of MRINs, we employed a mouse model of acute liver failure (Figure 4A,B). Liver failure was evident in mice that received injections of carbon tetrachloride (CCl_4) (Figure 4C), as there was a large area of necrosis and inflammation in the hepatic lobule center. Over the 2 weeks, intravenous MRIN therapy (red) significantly improved the survival of the animals, while NP therapy (green) and CM therapy (orange) only marginally improved the survival (Figure 4D). 12 h post-intravenous injection, MRINs or NPs can be detected in the lungs, livers, spleens, and kidneys of the treated animals (Figure 4E, middle). At 24 h, the signals in the lungs and kidneys decayed with increased signal in the livers (Figure 4E, right). At either time point, more MRINs than NPs were detected in the liver, suggesting the RBC coat on MRINs enhanced liver retention (Figure 4F). To increase the temporal resolution of biodistribution, we examined organ distributions of MRINs and NPs at an earlier time point (6 h). Interestingly, at 6 h, more NPs than MRINs were detected in liver, suggesting more rapid clearance of NPs by the liver macrophages (Figure 4E, left). This is consistent with the *in vitro* data presented in Figure 3. In addition, we examined the biodistribution of MRINs and NPs in normal mice (instead of liver failure mice). The organ pattern of biodistribution in normal mice was similar to that from liver failure mice (Supporting Information Figure S1A,B). At any given time point, the organ retention of MRINs in normal mice was similar to that in liver failure mice (Supporting Information Figure S1C).

MRIN Therapy Protects Liver Functions in CCl_4-Induced Liver Failure.

Alanine aminotransferase (ALT) and aspartate aminotransferase (AST) are excellent biomarkers for liver functions. At baseline, the ALT and AST levels were identical among all treatment groups, indicating a similar degree of initial injury by CCl_4 (Figure 5A,B, baseline). At 3 d and 7 d post-therapy, MRIN injections significantly reduced ALT and AST levels. Injection of NP or CM resulted in a certain degree of liver function protection as compared to the PBS control group. However, MRIN injection generated a larger therapeutic benefit than the CM or NP group. Injection of MRIN particles did not impair the kidney functions of the mice (Figure 5C,D). Interestingly, MRIN therapy effectively reduced the circulation levels of proinflammatory cytokines such as interleukin-6 (IL-6), interleukin-1 beta (IL-1β), and tumor necrosis factor-α (TNF-α) in the animals (Figure 5E− G), suggesting the anti-inflammatory role of MRIN therapy.

MRIN Therapy Reduces Apoptosis but Promotes Regeneration.

H&E staining indicated that MRIN therapy protected liver morphology (Figure 6A). Sham group showed normal hepatic lobule structures and portal area. Control group exhibited the sign of hepatic lobule structure disorder and hepatocellular edema. NP or CM treatment led to a certain degree of recovery in hepatic lobule structures. However, there was still a large number of inflammatory cell infiltration in the portal area. MRIN treatment led to the preservation of normal hepatic lobule structures. Ki67 staining revealed that MRIN

treatment promoted liver cell proliferation, suggesting higher levels of regeneration (Figure 6B,D). In addition, terminal deoxynucleotidyl transferase-mediated dUTP nick end labeling (TUNEL) staining revealed that MRIN injection was more potent than CM or NP therapy in reducing apoptosis in CCl_4-induced liver failure (Figure 6C,E).

DISCUSSION

In the present study, we fabricated a designer NP named MRIN by coating RBC cell membranes onto PLGA particles loaded with MSC secretome. This NP exhibited similar secretome as real MSCs and surface antigen profiles as RBCs. The advantages of our system are (1) the RBC membrane serves as the camouflage to protect the NP from recognition by macrophages; (2) the size of MRIN, 200 nm, is tailored to have great liver retention after intravenous delivery; and (3) unlike real MSCs, MRINs support long-term cryostorage after lyophilization.

Our previous work reported microsized synthetic MSC particles (MSC secretome + MSC membrane).[10] The rationale to use MRIN here is to increase stability and bioavailability to the liver after intravenous delivery: (1) microsized particles will be blocked by the lungs after intravenous delivery, therefore we designed MRIN as a NP; and (2) since MRIN will circulate in the blood, we adopted a (MSC secretome + RBC membrane) strategy for hemocompatibility.

MRIN is a product that integrates the principles of stem cell biology and nanomedicine. Cell therapy is a promising approach to liver regeneration. So far, multiple cell types, including MSCs, have been tested preclinically and clinically for treating liver diseases such as liver failure, liver fibrosis, or liver cirrhosis.[8,18,19] However, translation and efficacy are hindered by the intrinsic limitations of cellular products. Intravenously injected cells are filtered in the lungs and have difficulty reaching the liver. In addition, cell viability can rapidly decrease over the time during storage and shipping. These dead or dying cells can produce pro-death microvesicles to undermine the overall therapeutic benefits of the cell therapy. We took a biomimetic approach by creating polymer NPs that encapsulate the growth factors secreted by MSCs. Unlike real MSCs, these particles (~200 nm) are small enough to pass the lungs and reach the liver. In addition, since they are not real cells, they can be lyophilized and cryo-stored before usage. To make the NP more stable in the blood and in the liver, we cloak the NPs with the membranes of RBCs. The final product MRIN integrates the advantages of MSCs, RBCs, and NPs.

CCl_4-induced acute liver failure is a well-established model to study liver failure in humans.[20] We tested the therapeutic effects of NP (with MSC factors but without RBC coating), MRIN, and bare conditioned media from MSC in the same model. A PBS injection group was included as a negative control. The highest degree of therapeutic effects was seen in the MRIN-injected animals. We believe the higher retention of MRIN than NP in the liver is not due to active targeting but resulted from a longer blood half-life. MRIN has longer circulation time than NP. This resulted into a higher retention in the liver at 12 and 24 h. While NPs or bare conditioned media from MSCs can promote liver regeneration to a

certain degree, the regenerative effects are amplified by MRIN due to its excellent stability and longer blood half-life.

CONCLUSIONS

We found that intravenous injections of MRINs (a NP composed of MSC-secreted factors and RBC membranes) reduced the circulating levels of pro-inflammatory cytokines, decreased hepatic apoptosis, augmented liver regeneration and function, and eventually improved the survival rates of the mice in acute liver failure.

METHODS/EXPERIMENTAL

Preparation of MSC Conditioned Medium-Loaded PLGA NPs.

Human bone marrow-derived MSC was directly obtained from ATCC (cat no.: 63208778). The cells were cultured per vendor's instructions. Briefly, the MSCs were cultured in Iscove's modified Dulbecco's medium (IMDM, Thermo Fisher Scientific) for 3 days, and then the supernatant was collected to harvest conditioned media. Conditioned media was collected and filtered through a 0.22 μM filter into a sterile 50 mL conical to remove any cell debris and contaminants. Sterile conditioned media was stored at −80 °C for at least 24 h then lyophilized by a freeze-dry system. MSC conditioned media-loaded PLGA NPs were fabricated by a double emulsion process followed by membrane extrusion.[21] In brief, concentrated human MSC conditioned medium was prepared as the internal aqueous phase in poly(vinyl alcohol) (PVA) (0.1%) and injected into dichloromethane (DCM) containing polylactic-*co*-glycolic acid (PLGA). The whole content was then sonicated on ice for emulsification. Afterward, the emulsion was immediately transferred into water with PVA. The secondary emulsion was emulsified again to produce the final water/oil/water mixture. Then, it was stirred overnight to promote solvent evaporation. To enable detection, we prelabeled PLGA with Cy5.5 or AF594 fluorophore. The solidified NPs were then centrifuged and washed with water. The particles were then extruded through membranes with pore sizes of 400 and 200 nm using an extruder (Avanti Polar Lipids, Alabaster, AL).

Flow cytometry.

To characterize the phenotypes of MSC, flow cytometry was performed using a Beckman Coulter flow cytometer (Brea, CA). Primary antibodies used are CD31 (BD555445), CD34 (BD555821), CD45 (BD 555482), CD90 (BD 555595), and CD105 (FAB 10971P, R&D Systems) from BD company or R&D Systems.

Generation of RBC Membrane Vesicles.

The whole blood withdraws from C57BL/6 mice (6 weeks, 18−25 g, Charles River Laboratories) was centrifuged at 800 × *g* to obtain RBC pellets. The RBCs were then washed 3 times with cold PBS. After that, hemolysis was triggered by treatment with a hypotonic solution and subsequently centrifuged at 800 × *g* for 5 min. The resulting RBC shells (free of cytoplasmic components) were washed with PBS and examined using a white light microscope.[22] To prepare RBC membrane vesicles, RBC shells were subjected to three

freeze/thaw cycles. After that, the collected RBC shells were extruded through membranes with pore sizes of 400 and 200 nm using an extruder (Avanti Polar Lipids).

Fabrication and Characterization of MRIN.

To cloak the RBC vesicles onto the surface of MSC-NPs, 0.5 mL of MSC-NPs (5×10^9/ ml) was mixed with 0.5 mL RBC vesicles (5×10^9/ml) and then extruded 11 times as previously described. The resulting MRINs were centrifuged at 800 × *g* to remove excessive membrane debris. NP concentration and size were examined by NanoSight (Malvern, UK). Surface charge (ζ potential, mV) was measured by dynamic light scattering (DLS). The morphology of MRINs was studied by TEM (JEOL JEM-2000FX). The coated specimen was imaged after negative staining with 1 wt % uranyl acetate. To reveal whether MRINs have the same signature proteins as RBCs, SDS-PAGE was performed to reveal the protein components of RBC membrane vesicles and the dialyzed MRIN particles.

Growth Factors Release Study and Pharmacokinetic Studies *in Vivo*.

Total protein and growth factor releases from MRINs were determined as previously described.[10,23] In brief, freezedried MRINs were dissolved in DCM. After that, PBS was added to the solution. The sample was subjected to vortex for 5−10 min to isolate proteins from the oil phase to the water phase. After centrifugation, the protein concentration in the water phase was measured by a bicinchoninic acid assay. For growth factor release studies, NPs were incubated in PBS at 37 °C. The supernatant was collected at different time points (24, 48, 72, 96, 120, and 144 h), and the concentrations of various growth factors were determined by enzyme-linked immunosorbent assays (ELISAs). Ten male C57BL/6 mice were randomized into two groups ($n = 5$ per group) and were intravenously injected with NP and MRIN NPs (both labeled with Cy5.5 fluorophore during NP preparation). At 0.5, 1, 2, 4, 12, 24, and 48 h, 20 μL whole blood was collected. NP concentrations were determined by UV−vis spectra using a Nanodrop 2000 (Thermo Scientific, USA). Known concentrations of Cy5.5-labeled NPs were mixed with blood to generate a standard calibration curve. The concentrations of NPs in different blood samples were calculated based on the standard curve.

Macrophage Uptake Study.

Human peripheral blood mononuclear cells (hPBMCs) were isolated from healthy volunteers. A Ficoll separation method was followed. CD14+ cells were purified by magnetic-activated cell sorting using CD14+ selection magnetic beads (Stem Cell Technologies) and differentiated to macrophages, using RPMI media supplemented with 1% glutamine and 10% human serum.[24] M1 macrophages were enriched with further polarization using 100 ng/nl of LPS (Sigma) and IFN-r (Peprotech). At day 7, M1 macrophages were co-incubated with RBC-coated MRINs or uncoated control NPs at 37 °C for 3 h and then washed with PBS for 3 times for imaging. For imaging purposes, both MRINs and NPs were prelabeled with AF594 fluorophore. After the co-incubation period, cells were fixed with 4% glutaraldehyde at room temperature, counterstained with DAPI before microscopic imaging.

In Vitro Cell-Based Assays.

The immortalized liver cell line (THLE-2) was obtained from ATCC (CRL-2706) and cultured in a BEGM Bullet Kit (Lonza, CC3170) supplementation with 70 ng/mL phosphoethanolamine (Sigma, P0503), 5 ng/mL EGF (Sigma, E5036), and 10% fetal calf serum superior (Sigma). HSC-T6 cell line was obtained from Sigma (SCC069) and cultured in IMDM media (Invitrogen, Carlsbad, CA) with 10% FBS (Corning), 0.5% gentanicin, 0.1 mM 2-mercaptoethanol, and 1% L-glutamine. Primary mouse lung cells were obtained and maintained with the lung spheroid methods as previously described.[25–27] To mimic liver injury, all cells were incubated with 20 mmol/mL CCl_4 for 24 h. After that, the cells were further incubated with different concentration of MRINs for 24 h. A Cell Counting Kit-8 (CCK-8, 96992 Sigma) was used to evaluate cell proliferation.

Ex Vivo Fluorescent Imaging for Biodistribution of MRINs.

Cohorts of normal mice and liver failure mice were scarified 6, 12, and 24 h after NP injections; major organs were collected for biodistribution studies using *ex vivo* fluorescent imaging (IVIS, Caliper Lifesciences, Waltham, MA).

Mouse Model of Acute Liver Failure and MRIN Therapy.

All animal work was compliant with the IACUC at North Carolina State University. Briefly, C57BL/6 mice (body weight 18−25g) were anesthetized with isofluorane inhalation. Then, 4.0 mL/kg CCl_4 (Sigma, 2891116) mixed with olive oil (Sigma, O1514) (1:1 ratio) was injected intraperitoneally. After 24 h, the liver failure model was confirmed by histology. After that, the mice were randomized into the following treatment arms: (1) Sham group: no liver failure induction or therapy; (2) PBS control group: liver failure + tail vein injection of 200 μL PBS to the liver failure mice; (3) CM group: liver failure + tail vein injection of 1 mg CM lyophilized powder dissolved in 200 μL PBS; (4) NP group: liver failure + tail vein injection of 1×10^9 NPs in 200 μL PBS; (5) MRIN group: tail injection of 1×10^9 MRINs in 200 μL. The mice were given the injections twice a week for 2 weeks (total 4 injections).

Liver/Kidney Function Test and Cytokine Assay.

Liver and kidney functions were examined by measuring serum ALT and AST levels, blood urea nitrogen (BUN), and creatinine (Cr) by the veterinary hospital of NC State University. The serum levels of IL-1β (Sigma, RAB0275), IL-6 (Sigma, RAB0308), and TNF-α (Sigma, RAB0477) were measured with commercially available ELISAs. Survival rates were analyzed using a Kaplan−Meier plot with log-rank analysis.

Histology.

Liver tissues were kept in 10% formalin and embedded in paraffin. After cutting, liver sections (5 μm thick) were subjected to hematoxylin and eosin (H&E) staining. Images were taken by a microscopy (AZ-100). For immunohistochemistry, 10 μm-thick liver cryo-sections were fixed with 4% paraformaldehyde (PFA) and permeabilized/blocked. The slides were then incubated with rabbit anti-Ki67 (1:100, ab15580, Abcam) overnight at 4 °C. After that the cells were incubated with Texas-Red secondary antibodies (1:100, ab6719, Abcam) and counterstained with DAPI. For assessment of cell apoptosis, liver cryo-sections were

incubated with TUNEL solution (Roche Diagnostics, Germany) and counterstained with DAPI. To study the cellular location of MRINs in the liver, liver cryosections were incubated with anti-WGA (1:50, ab20528, abcam) for liver cells and anti-CD45(1:200, ab10558, abcam) for macrophages, followed by incubation with AF488 secondary antibodies (1:200, ab150077, abcam). Images were taken by a confocal microscope (Carl Zeiss, Germany).

Statistical Analysis.

All data were presented as the mean ± SD. Two-tailed Student's *t* test was used for comparison between two groups. Comparisons among three or more groups were performed using one-way ANOVA. Statistical significance was considered when $P < 0.05$.

Supplementary Material

Refer to Web version on PubMed Central for supplementary material.

ACKNOWLEDGMENTS

This work was supported by funding from National Institute of Health (HL123920, HL137093), NC State University Chancellor's Faculty Excellence Program, NC State Chancellor's Innovation Fund, a University of North Carolina General Assembly Research Opportunities Initiative grant, Scientific and Technological Project of Henan Province, China (152102410063), and Henan Province Commission of Heath and Family Planning (2015027).

REFERENCES

(1). Elias E Liver Failure and Liver Disease. Hepatology 2006, 43, S239–242. [PubMed: 16447294]

(2). Starzl TE The Long Reach of Liver Transplantation. Nat. Med 2012, 18, 1489–1492. [PubMed: 23042359]

(3). Jalan R; Gines P; Olson JC; Mookerjee RP; Moreau R; Garcia-Tsao G; Arroyo V; Kamath PS Acute-on Chronic Liver Failure. J. Hepatol 2012, 57, 1336–1348. [PubMed: 22750750]

(4). Itoh T; Miyajima A Liver Regeneration by Stem/Progenitor Cells. Hepatology 2014, 59, 1617–1626. [PubMed: 24115180]

(5). Zhang Z; Wang FS Stem Cell Therapies for Liver Failure and Cirrhosis. J. Hepatol 2013, 59, 183–185. [PubMed: 23353868]

(6). Li J; Zhang L; Xin J; Jiang L; Li J; Zhang T; Jin L; Li J; Zhou P; Hao S; Cao H; Li L Immediate Intraportal Transplantation of Human Bone Marrow Mesenchymal Stem Cells Prevents Death from Fulminant Hepatic Failure in Pigs. Hepatology 2012, 56, 1044–1052. [PubMed: 22422600]

(7). Shi D; Zhang J; Zhou Q; Xin J; Jiang J; Jiang L; Wu T; Li J; Ding W; Li J; Zhou N; Zhang L; Jin L; Hao S; Chen P; Cao H; Li M; Li L; et al. Quantitative Evaluation of Human Bone Mesenchymal Stem Cells Rescuing Fulminant Hepatic Failure in Pigs. Gut 2017, 66, 955–964. [PubMed: 26884426]

(8). Lin BL; Chen JF; Qiu WH; Wang KW; Xie DY; Chen XY; Liu QL; Peng L; Li JG; Mei YY; Weng WZ; Peng YW; Cao HJ; Xie JQ; Xie SB; Xiang AP; Gao ZL Allogeneic Bone Marrow-Derived Mesenchymal Stromal Cells for Hepatitis B Virus-Related Acute-On-Chronic Liver Failure: A Randomized Controlled Trial. Hepatology 2017, 66, 209–2019. [PubMed: 28370357]

(9). Chen L; Xiang B; Wang X; Xiang C Exosomes Drived from Human Menstrual Blood-Derived Stem Cells Alleviate Fulmiant Hepatic Failure. Stem Cell Res. Ther 2017, 8, 9.

(10). Luo L; Tang J; Nishi K; Yan C; Dinh PU; Cores J; Kudo T; Zhang J; Li TS; Cheng K Fabrication of Synthetic Mesenchymal Stem Cells for the Treatment of Acute Myocardial Infarction in Mice. Circ. Res 2017, 120, 1768–1775. [PubMed: 28298296]

(11). Hu CM; Zhang L; Aryal S; Cheung C; Fang RH; Zhang L Erythrocyte Membrane-Camouflaged Polymeric Nanoparticles as a Biomimetic Delivery Platform. Proc. Natl. Acad. Sci. U. S. A 2011, 108, 10980–10985. [PubMed: 21690347]

(12). Hu CM; Fang RH; Wang KC; Luk BT; Thamphiwatana S; Dehaini D; Nguyen P; Angsantikul P; Wen CH; Kroll AV; Carpenter C; Ramesh M; Qu V; Patel SH; Zhu J; Shi W; Hofman FM; Chen TC; Gao W; Zhang K; et al. Nanoparticle Biointerfacing by Platelet Membrane Cloaking. Nature 2015, 526, 118–121. [PubMed: 26374997]

(13). Sun H; Su J; Meng Q; Yin Q; Chen L; Gu W; Zhang P; Zhang Z; Yu H; Wang S; Li Y Cancer-Cell-Biomimetic Nanoparticles for Targeted Therapy of Homotypic Tumors. Adv. Mater 2016, 28, 9581–9588. [PubMed: 27628433]

(14). Fang RH; Hu CM; Luk BT; Gao W; Copp JA; Tai Y; O'Connor DE; Zhang L Cancer Cell Membrane-Coated Nanoparticles for Anticancer Vaccination and Drug Delivery. Nano Lett 2014, 14, 2181–2188. [PubMed: 24673373]

(15). Hu Q; Sun W; Qian C; Wang C; Bomba HN; Gu Z Anticancer Platelet-Mimicking Nanovehicles. Adv. Mater 2015, 27, 7043–7050. [PubMed: 26416431]

(16). Mohandas N; Gallagher PG Red Cell Membrane: Past, Present, and Future. Blood 2008, 112, 3939–3948. [PubMed: 18988878]

(17). Piao JG; Wang L; Gao F; You YZ; Xiong Y; Yang L Erythrocyte Membrane is An Alternative Coating To Polyethylene Glycol for Prolonging the Circulation Lifetime of Gold Nanocages for Photothermal Therapy. ACS Nano 2014, 8, 10414–10425. [PubMed: 25286086]

(18). Zhang Y; Cai W; Huang Q; Gu Y; Shi Y; Huang J; Zhao F; Liu Q; Wei X; Jin M; Wu C; Xie Q; Zhang Y; Wan B; Zhang Y Mesenchymal Stem Cells Alleviate Bacteria-Induced Liver Injury in Mice by Inducing Regulatory Dendritic Cells. Hepatology 2014, 59, 671–682. [PubMed: 23929707]

(19). El Agha E; Kramann R; Schneider RK; Li X; Seeger W; Humphreys BD; Bellusci S Mesenchymal Stem Cells in Fibrotic Disease. Cell Stem Cell 2017, 21, 166–177. [PubMed: 28777943]

(20). Nagamoto Y; Takayama K; Ohashi K; Okamoto R; Sakurai F; Tachibana M; Kawabata K; Mizuguchi H Transplantation of a Huma Ipsc-Derived Hepatocyte Sheet Increases Survival in Mice with Acute Liver Failure. J. Hepatol 2016, 64, 1068–1075. [PubMed: 26778754]

(21). Zhai Y; Su J; Ran W; Zhang P; Yin Q; Zhang Z; et al. Preparation and Application of Cell Membrane-Camouflaged Nanoparticles for Cancer Therapy. Theranostics 2017, 7, 2575–2592. [PubMed: 28819448]

(22). Gao W; Hu CM; Fang RH; Luk BT; Su J; Zhang L Surface Functionalization of RBC Membrane Vesicles Gold Nanoparticles with Red Blood Cell Membranes. Adv. Mater 2013, 25, 3549–3553. [PubMed: 23712782]

(23). Tang J; Shen D; Caranasos TG; Wang Z; Vandergriff AC; Allen TA; Hensley MT; Dinh PU; Cores J; Li TS; Zhang J; Kan Q; Cheng K Therapeutic Microparticles Function-alized with Biomimetic Cardiac Stem Cell Membranes and Secretome. Nat. Commun 2017, 8, 13724. [PubMed: 28045024]

(24). Pallotta I; Sun B; Wrona EA; Freytes DO BMP Protein-Mediated Crosstalk Between Inflammatory Cells and Human Pluripotent Stem Cell-Derived Cardiomyocytes. J. Tissue Eng. Regener. Med 2017, 11, 1466–1478.

(25). Cores J; Hensley MT; Kinlaw K; Rikard SM; Dinh PU; Paudel D; Tang J; Vandergriff AC; Allen TA; Li Y; Liu J; Niu B; Chi Y; Caranasos T; Lobo LJ; Cheng K Safety and Efficacy of Allogeneic Lung Spheroid Cells in a Mismatched Rat Model of Pulmonary Fibrosis. Stem Cells Transl. Med 2017, 6, 1905–1916. [PubMed: 28783251]

(26). Dinh PC; Cores J; Hensley MT; Vandergriff AC; Tang J; Allen TA; Caranasos TG; Adler KB; Lobo LJ; Cheng K Derivation of Therapeutic Lung Spheroid Cells from Minimally Invasive Transbronchial Pulmonary Biopsies. Respir. Res 2017, 18, 132. [PubMed: 28666430]

(27). Henry E; Cores J; Hensley MT; Anthony S; Vandergriff A; de Andrade JBM; Allen T; Caranasos TG; Lobo LJ; Cheng K Adult Lung Spheroid Cells Contain Progenitor Cells and Mediate Regeneration in Rodents with Bleomycin-Induced Pulmonary Fibrosis. Stem Cells Transl. Med 2015, 4, 1265–1274. [PubMed: 26359426]

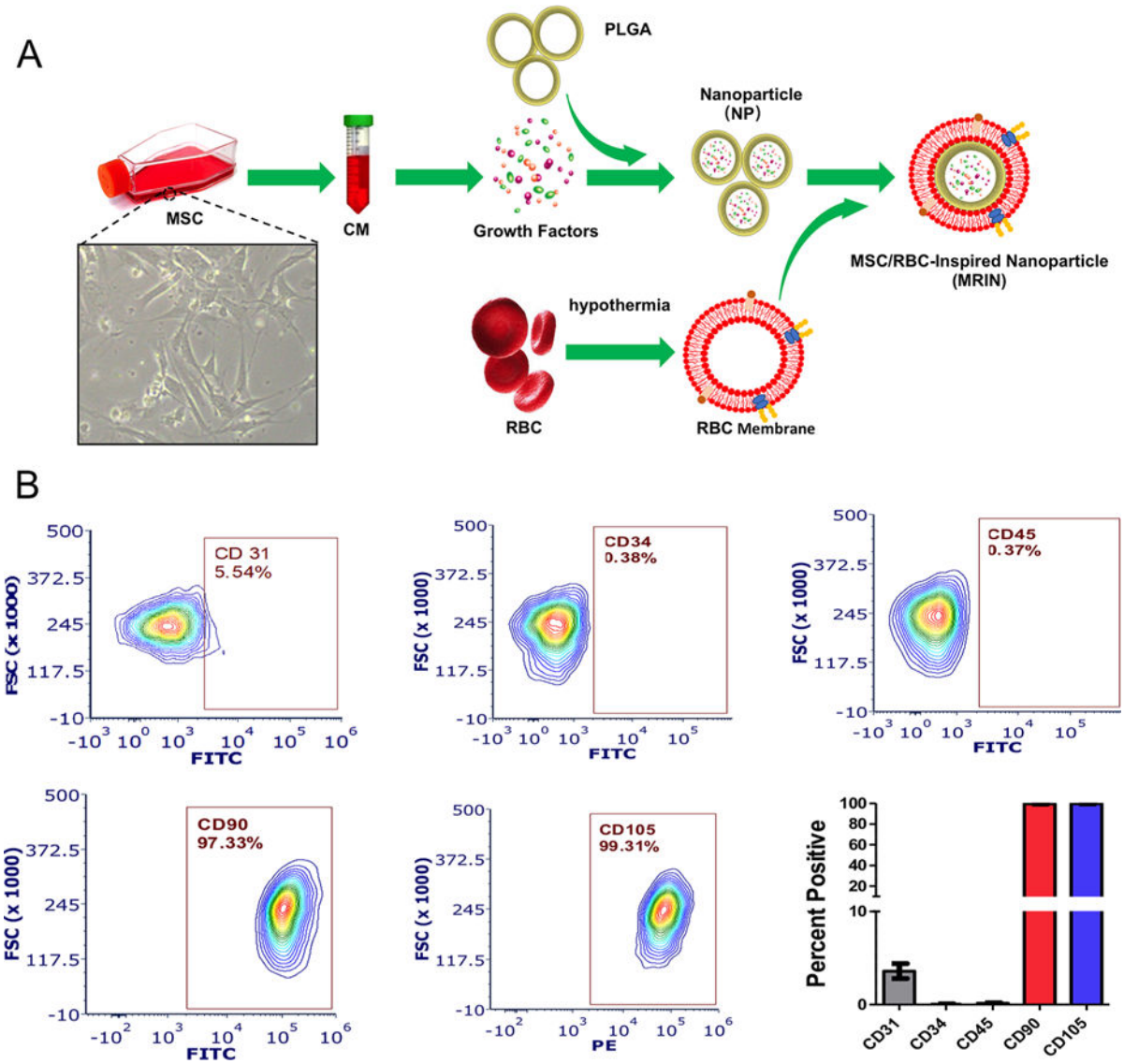

Figure 1.

Characterization MSCs and fabrication of MRINs. (A) Schematic illustration showing the fabrication of MRINs involves three steps: preparation of membrane vesicles from RBCs; preparation of NPs from MSC-conditioned media, and cloaking of RBC membranes on NPs to make MRINs. (B) Flow cytometry analysis of common MSC markers such as CD105, CD90, CD45, CD31, and CD34 ($n = 3$ for each marker).

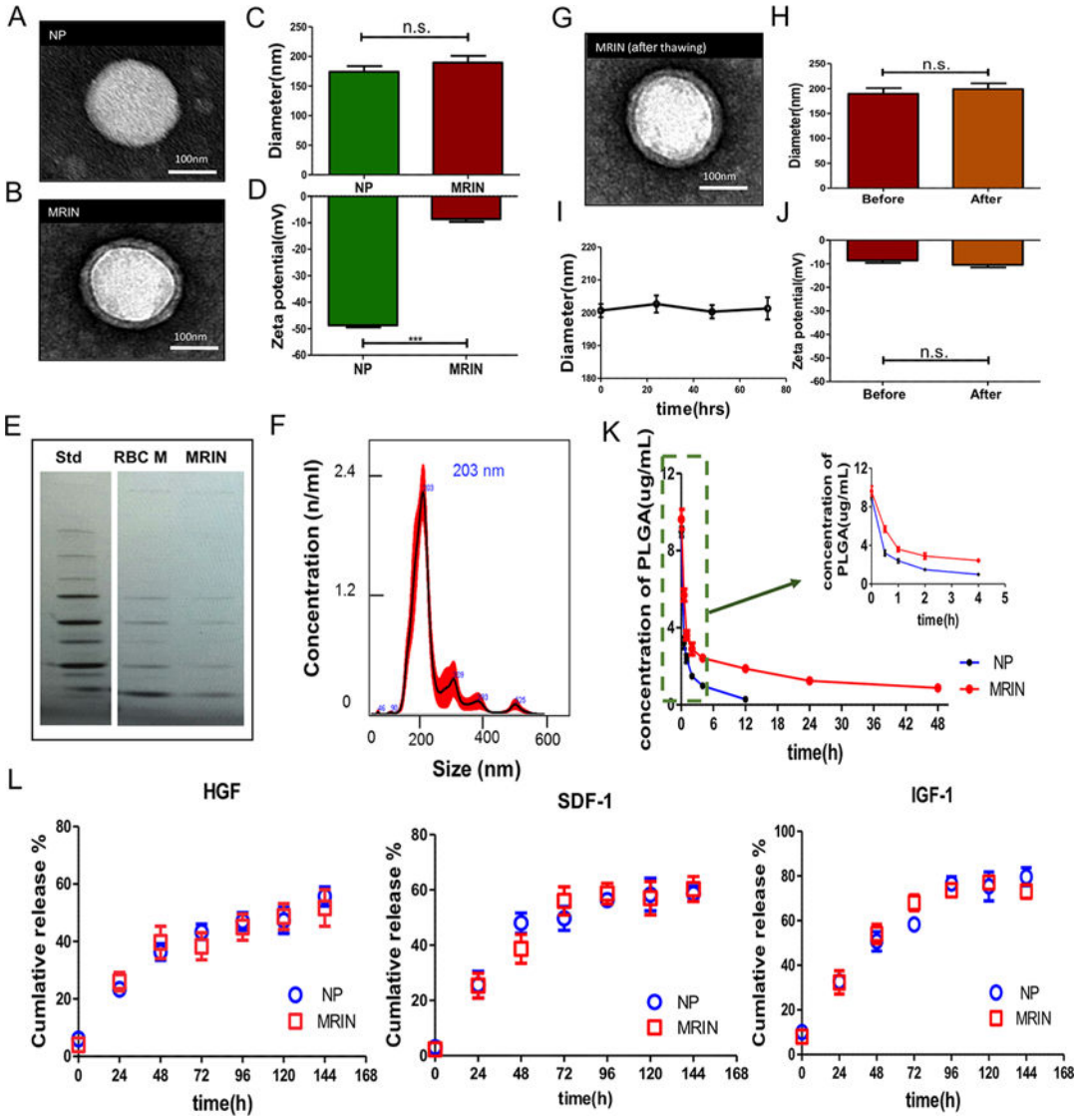

Figure 2.

Physiochemical and biological properties of MRINs. (A, B) TEM images of a NP and a MRIN. The NPs were negatively stained with uranyl acetate and subsequently visualized with TEM. (C) Diameters (nm) of NPs and MRINs measured by NanoSight ($n = 4$). (D) Zeta potential (mV) of NPs and MRINs ($n = 3$). (E) Images of SDS-PAGE gels examining protein contents of MRIN, which have similar protein bands as those observed from RBC membranes. (F) Size distribution of MRIN measured by NanoSight. The average size is approximately 200 nm. (G) A TEM image of a MRIN after freeze/thaw, showing the RBC coat is still intact. (H) Diameters (nm) of MRIN before and after freeze/thaw ($n = 4$). (I) Size change of MRINs after storage at room temperature ($n = 3$ for each time point). (J) Zeta potential (mV) of MRIN before and after freeze/thaw ($n = 3$). (K) Blood retentions of NPs and MRINs over a span of 48 h ($n = 5$). (L) Quantitative analyses on the releases of stromal cell-derived factor-1 (SDF-1), insulin-like growth factor-1 (IGF-1), and hepatocyte growth factor (HGF) from NPs and MRINs over time; n.s. indicated $P > 0.05$. Comparisons between

any two groups were performed using two-tailed unpaired Student's *t* test. Scale bars, 100 nm. All data are expressed the means ± SD.

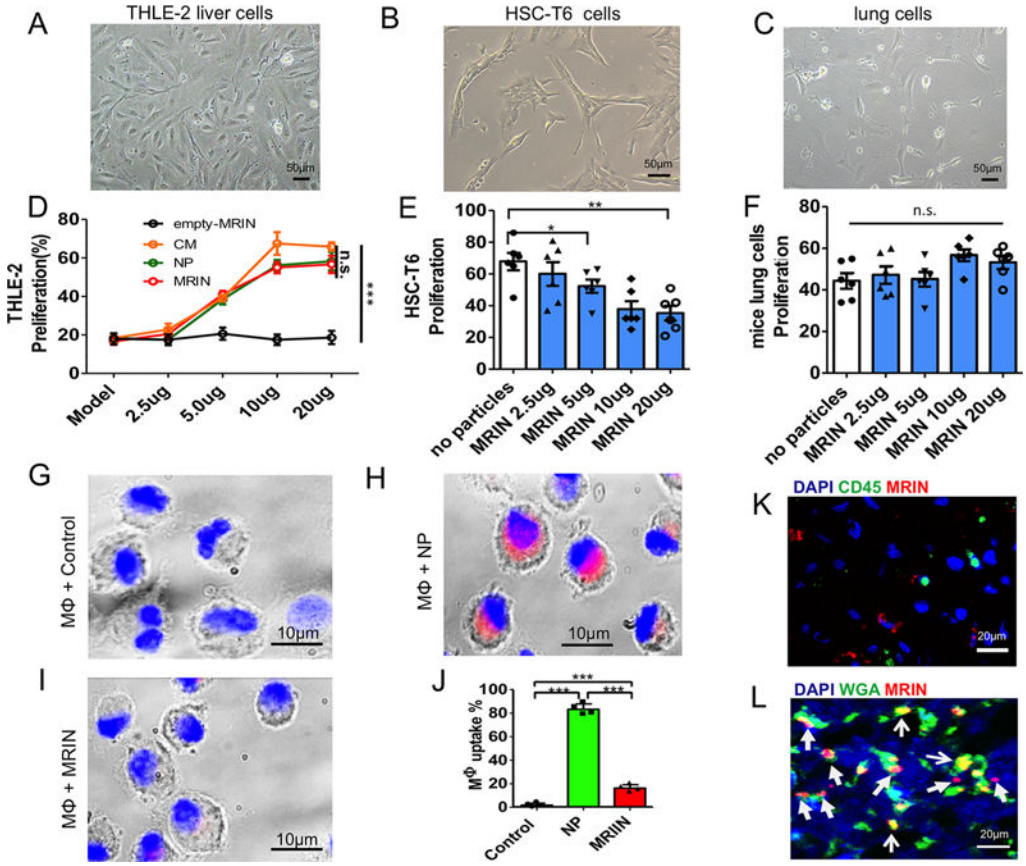

Figure 3.

Effects of MRINs on liver, lung, and M1 macrophage cells. (A, B, C) Morphology of THLE-2 cells, HSC-T6 cells, and mouse lung cells indicated by white light microscopy. Scale bars, 50 μm. (D) Percentages of proliferating THLE-2 cells under various treatments ($n = 6$ for each group). (E, F) Proliferation of HSC-T6 cells and mouse lung cells under various concentrations of MRINs ($n = 6$ for each group). (G−I) Macrophage uptake of NPs and MRINs (red) after 3 h of co-incubation. Scale bars, 10 μm. (J) Quantitative analysis of the percentages of macrophages with particle endocytosis ($n = 4$ for each group). (K) Representative confocal microscopy image showing the minimal internalization of MRINs (red) by liver macrophages (green; stained with CD45). Scar bar, 20 μm. (L) Representative confocal microscopy image showing the location of MRINs (red) relative to liver cells (green; stained with WGA). Scar bar, 20 μm. * indicates $P < 0.05$; ** indicates $P < 0.01$; *** indicates $P < 0.0001$; n.s. indicated $P > 0.05$. Student's t-test for comparison between two groups and one-way ANOVA for comparison among three and more groups. All data are expressed the means ± SD.

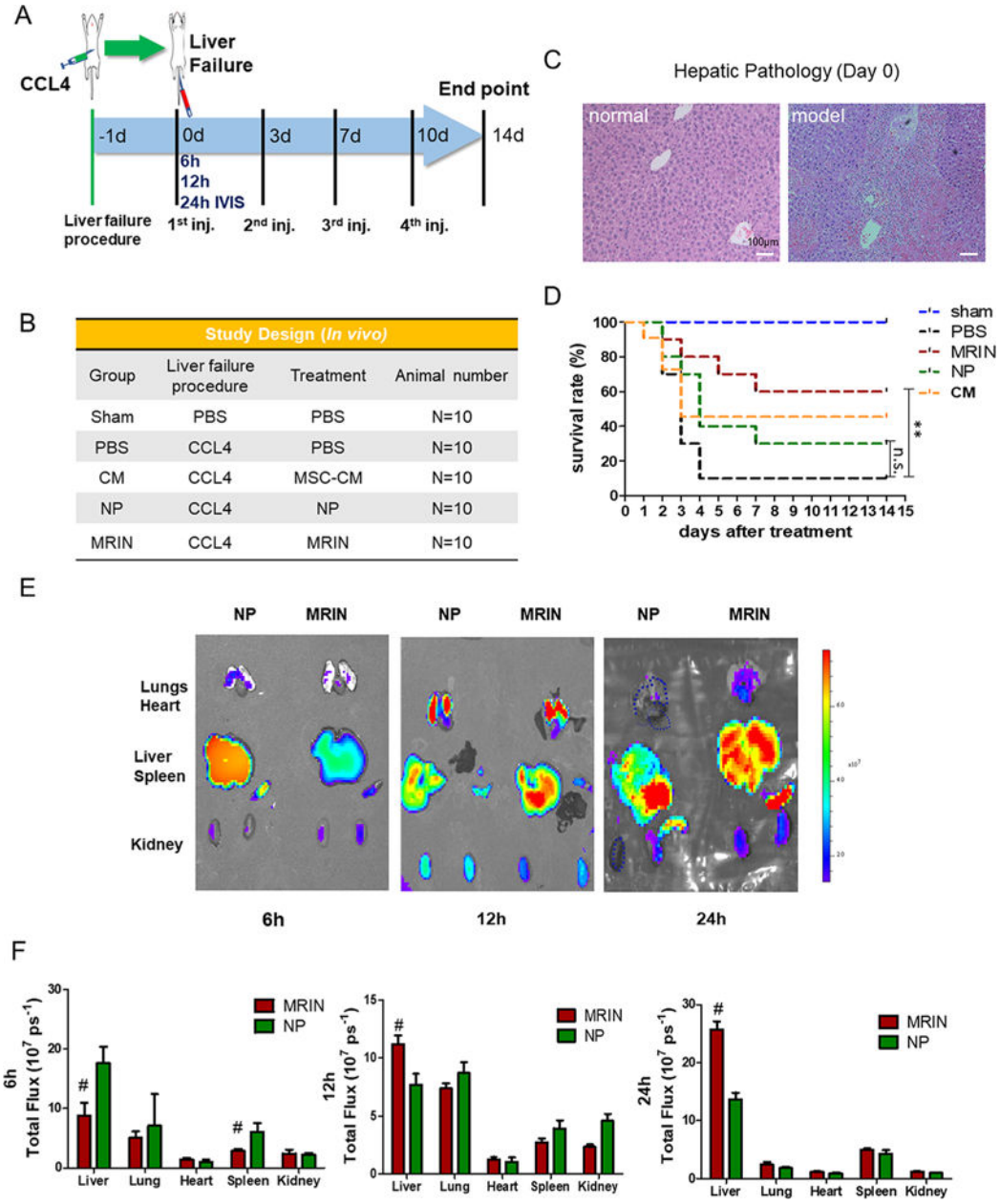

Figure 4.

Biodistrbution of MRINs and effects on animal survival. (A) Schematic showing the animal study design. (B) A tabular summary of study groups. (C) Liver histology after CCl_4 treatment. H&E staining showing confluent necrosis of the hepatic lobules in model mice but not in normal mice. (D) Survival rates of animal in various groups ($n = 10$ animals per group). (E) Biodistributions of NPs and MRINs after systemic administration in mice with acute liver failure. Representative *ex vivo* fluorescent imaging of mouse organs (heart, lungs, liver, spleen and kidneys) at 6, 12, and 24 h post-intravenous NP and MRIN injections. (F) Quantitative analysis of fluorescent intensities ($n = 3$ animals per group). # indicates $P <$ 0.01 when compared to NP group. Student's *t*-test for comparison between two groups and

one-way ANOVA for comparison among three and more groups. All data are expressed the means ± SD.

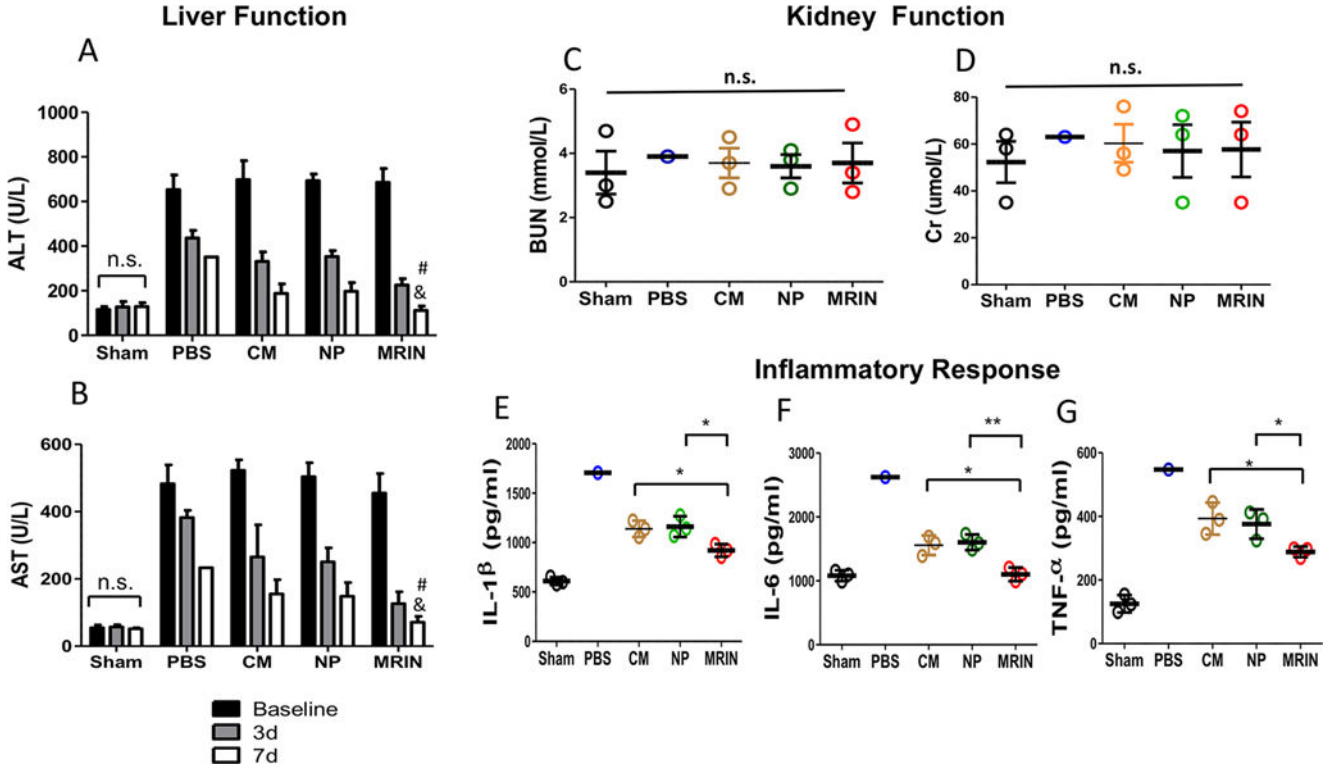

Figure 5.

MRIN therapy improves liver function and reduces systemic inflammation. (A, B) Serum levels of ALT and AST were measured 24 h after CCl_4 injection (baseline) and 3 or 7 days after treatment ($n = 3$ for each group). # indicates $P < 0.05$ when compared with NP group; and indicates $P < 0.05$ when compared with CM group. (C, D) Serum levels of BUN and Cr measured 2 weeks after therapy ($n = 1$ for PBS group and $n = 3$ for other groups). (E−G) Serum levels of IL-1β, IL-6, and TNF-α measured 2 weeks after therapy ($n = 1$ for PBS group and $n = 3$ for other groups). * indicates $P < 0.05$; ** indicates $P < 0.01$; n.s. indicated $P > 0.05$. Student's t-test for comparison between two groups and one-way ANOVA for comparison among three and more groups. All data are presented as mean ± SD.

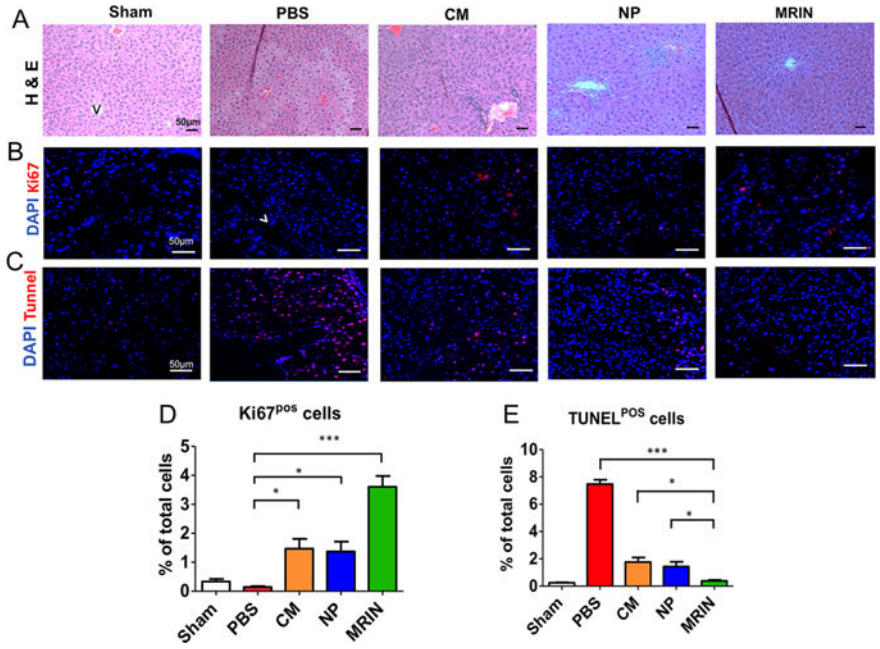

Figure 6.

MRIN therapy promotes liver cell regeneration and inhibits cell death. (A) H&E staining of liver sections from different groups. Scale bars, 50 μm. (B) Representative fluorescent micrographs showing Ki67-positive cells (red nuclei). Scale bars, 50 μm. (C) Representative fluorescent micrographs showing TUNEL-positive cells (red nuclei). Scale bars, 50 μm. (D, E) Quantitation of proliferative and apoptotic cells ($n = 3$ for each group). * indicates $P < 0.05$; *** indicated $P < 0.001$. Student's t-test for comparison between two groups and one-way ANOVA for comparison among three and more groups. All data are expressed the means ± SD.